

Homo sapiens reached the higher latitudes of Europe by 45,000 years ago

<https://doi.org/10.1038/s41586-023-06923-7>

Received: 27 June 2023

Accepted: 30 November 2023

Published online: 31 January 2024

Open access

 Check for updates

Dorothea Mylopotamitaki^{1,2,24}, Marcel Weiss^{2,3,24}✉, Helen Fewlass^{2,4,24}, Elena Irene Zavala^{2,5,24}, Hélène Rougier⁶, Arev Pelin Sümer², Mateja Hajdinjak², Geoff M. Smith^{2,7}, Karen Ruebens^{1,2}, Virginie Sinet-Mathiot^{2,8}, Sarah Pederzani^{2,9}, Elena Essel², Florian S. Harking¹⁰, Huan Xia¹¹, Jakob Hansen^{12,13}, André Kirchner¹⁴, Tobias Lauer^{2,15}, Mareike Stahlschmidt^{2,16}, Michael Hein^{2,17,18}, Sahra Talamo^{2,19}, Lukas Wacker²⁰, Harald Meller²¹, Holger Dietl²¹, Jörg Orschiedt²¹, Jesper V. Olsen¹⁰, Hugo Zeberg^{2,22}, Kay Prüfer², Johannes Krause², Matthias Meyer², Frido Welker¹², Shannon P. McPherron², Tim Schüller²³ & Jean-Jacques Hublin^{1,2}✉

The Middle to Upper Palaeolithic transition in Europe is associated with the regional disappearance of Neanderthals and the spread of *Homo sapiens*. Late Neanderthals persisted in western Europe several millennia after the occurrence of *H. sapiens* in eastern Europe¹. Local hybridization between the two groups occurred², but not on all occasions³. Archaeological evidence also indicates the presence of several technocomplexes during this transition, complicating our understanding and the association of behavioural adaptations with specific hominin groups⁴. One such technocomplex for which the makers are unknown is the Lincombian–Ranisian–Jerzmanowician (LRJ), which has been described in northwestern and central Europe^{5–8}. Here we present the morphological and proteomic taxonomic identification, mitochondrial DNA analysis and direct radiocarbon dating of human remains directly associated with an LRJ assemblage at the site Ilsenhöhle in Ranis (Germany). These human remains are among the earliest directly dated Upper Palaeolithic *H. sapiens* remains in Eurasia. We show that early *H. sapiens* associated with the LRJ were present in central and northwestern Europe long before the extinction of late Neanderthals in southwestern Europe. Our results strengthen the notion of a patchwork of distinct human populations and technocomplexes present in Europe during this transitional period.

The Middle to Upper Palaeolithic LRJ^{9,10} technocomplex extends across northwestern and central Europe (Fig. 1b and Supplementary Fig. 1a). It has been attributed to either Neanderthals⁵ or *H. sapiens*¹¹. Based on its stone tools, the LRJ has often been classified as Early Upper Palaeolithic¹² given the laminar blank production directed towards the production of partial-bifacial blade points (Jerzmanowice points)¹². By contrast, the LRJ has alternatively been interpreted as a local development by Neanderthals^{5,10}, as the bi-directional blade production differs from the predominantly uni-directional blade production system of the succeeding Upper Palaeolithic made by *H. sapiens*. Additionally,

the occasional presence of bifacial leaf points in some LRJ assemblages suggested a Middle Palaeolithic origin. From a chronological perspective, either attribution is possible, as LRJ assemblages are generally dated to about 44,000–41,000 calibrated years before the present (cal BP)^{5,13}, a period during which Neanderthals and *H. sapiens* groups are known to be present in Europe^{14–16}.

The site Ilsenhöhle in Ranis (50° 39.7563' N, 11° 33.9139' E, hereafter Ranis) is one of the eponymous LRJ sites based on its unique composition of bifacial and unifacial points. Ranis is located in the Orla River valley (Thuringia, Germany; Fig. 1b and Supplementary Fig. 1a).

¹Chair of Paleoanthropology, CIRB (UMR 7241–U1050), Collège de France, Paris, France. ²Max Planck Institute for Evolutionary Anthropology, Leipzig, Germany. ³Friedrich-Alexander-Universität Erlangen-Nürnberg, Institut für Ur- und Frühgeschichte, Erlangen, Germany. ⁴Ancient Genomics Lab, Francis Crick Institute, London, UK. ⁵Department of Molecular and Cell Biology, University of California Berkeley, Berkeley, CA, USA. ⁶Department of Anthropology, California State University Northridge, Northridge, CA, USA. ⁷School of Anthropology and Conservation, University of Kent, Canterbury, UK. ⁸Univ. Bordeaux, CNRS, Ministère de la Culture, PACEA, UMR 5199, Bordeaux, France. ⁹Archaeological Micromorphology and Biomarker Lab, University of La Laguna, San Cristóbal de La Laguna, Spain. ¹⁰Center for Protein Research, University of Copenhagen, Copenhagen, Denmark. ¹¹College of Earth and Environmental Sciences, Lanzhou University, Lanzhou, China. ¹²Globe Institute, University of Copenhagen, Copenhagen, Denmark. ¹³Departament de Prehistòria, Universitat Autònoma de Barcelona, Barcelona, Spain. ¹⁴Department of Soil Protection and Soil Survey, State Authority for Mining, Energy and Geology of Lower Saxony (LBEG), Hannover, Germany. ¹⁵Terrestrial Sedimentology, Department of Geosciences, University of Tübingen, Tübingen, Germany. ¹⁶Department of Evolutionary Anthropology and Human Evolution and Archaeological Sciences (HEAS), University of Vienna, Vienna, Austria. ¹⁷Institute of Ecology, Leuphana University, Lüneburg, Germany. ¹⁸Historical Anthropospheres Working Group, Leipzig Lab, Leipzig University, Leipzig, Germany. ¹⁹Department of Chemistry G. Ciamician, Bologna University, Bologna, Italy. ²⁰Ion Beam Physics, ETH Zurich, Zurich, Switzerland. ²¹Landesamt für Denkmalpflege und Archäologie Sachsen-Anhalt – Landesmuseum für Vorgeschichte, Halle, Germany. ²²Department of Physiology and Pharmacology, Karolinska Institutet, Stockholm, Sweden. ²³Thuringian State Office for the Preservation of Historical Monuments and Archaeology, Weimar, Germany. ²⁴These authors contributed equally: Dorothea Mylopotamitaki, Marcel Weiss, Helen Fewlass, Elena Irene Zavala. ✉e-mail: marcel.weiss@fau.de; hublin@eva.mpg.de

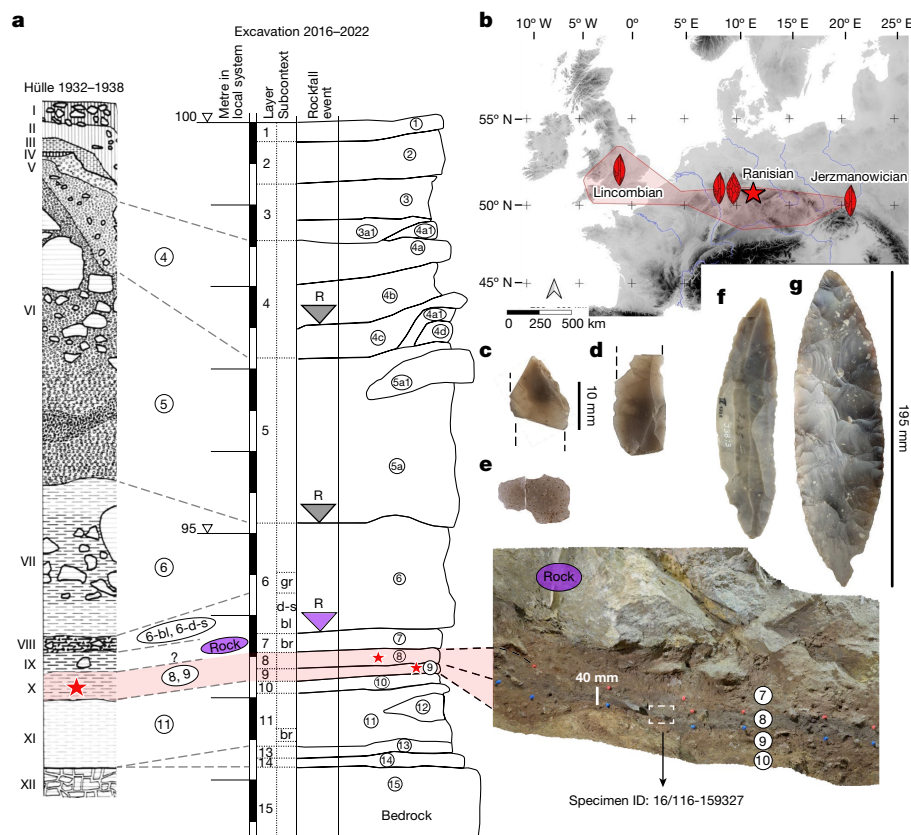


Fig. 1 | Stratigraphy with location of *H. sapiens* bones, map of LRJ sites and lithics from Ranis. a, General stratigraphy and correlations of the 1930s and 2016–2022 excavations with the in situ location of the hominin specimen ID 16/116-159327 within the layer 8, north profile (photograph). Stars mark the layers with hominin bones. Shaded in red are the LRJ layers. ‘R’ marks rockfall events. The purple rock represents the 1.7-m-thick rock that sealed the basal sequence. gr, grey; d-s, dark-spotted; bl, black; br, brown. **b**, Location of Ranis (star) and the LRJ (red shaded area). Schematic artefacts mark the dominant leaf

point type in the LRJ subdivisions (Lincombian (blade points), Ranisian (blade points and large bifacial points) and Jerzmanowician (blade points)). The map was created in QGIS³⁹ on the basis of Shuttle Radar Topography Mission data V4 (<http://srtm.csi.cgiar.org>)⁴⁰. **c, d**, Blade fragments (16/116-159048 and 16/116-151453), layer 8. **e**, Quartzite flake (16/116-159051) from surface retouch, layer 8. **f**, Jerzmanowice blade point, layer X (Museum Burg Ranis, IV 1328). **g**, Bifacial leaf point (Museum Burg Ranis IV 1319), layer X. **a**, Adapted from ref. 17. **f, g**, Photos: J. Schubert.

The cave formed in the south-facing cliff of a Permian limestone reef (Extended Data Fig. 1a and Supplementary Fig. 2a). Only two short chambers remain intact from a formerly large and high chamber that collapsed during the late Pleistocene¹⁷. Fieldwork started in 1926, continuing in 1929 and 1931, but the site was mainly excavated by W. M. Hülle between 1932 and 1938 (Extended Data Figs. 1b and 2 and Supplementary Fig. 3; ref. 17). Near the base of the 8-m sequence, these excavations revealed a complex stratigraphy of five layers (from bottom to top: XI to VII), including a layer (variably named X and Graue Schicht; Fig. 1a) rich in bifacial leaf points (Fig. 1g and Supplementary Fig. 2c) and with Jerzmanowice blade points (Fig. 1f and Supplementary Fig. 2d). This layer represents the Ranisian as part of the LRJ.

In 2016, we returned to Ranis to clarify the stratigraphy and chronology¹⁸ and to identify the makers of the LRJ. We reopened the main 1934 trench and excavated adjacent squares to bedrock (Extended Data Fig. 1b and Supplementary Figs. 2b and 3–8). Among the basal layers, layer 11 (Hülle: XI, Fig. 1a) has a low density of undiagnostic, possibly Middle Palaeolithic artefacts¹⁷. The overlying layer 10 has no equivalent in the 1932–1938 stratigraphy and is followed by layers 9 and 8, which we correlate with the LRJ layer X or Graue Schicht of the Hülle excavation (Fig. 1a). The following layer 7 is sealed by a roof collapse event. A large rock of 1.7 m thickness (Extended Data Fig. 1c and Supplementary Figs. 6 and 8) separates layer 7 from layer 6-black/dark spotted (Hülle: VIII), which contains younger Upper Palaeolithic artefacts. This

large rock prevented Hülle from excavating the key basal layers in this location (Extended Data Fig. 1b).

The correlation of our layers 9–8 with the LRJ layer X of the Hülle excavation is based on an extensive set of radiocarbon dates from both collections, ancient DNA analysis, sedimentology and micro-morphology showing anthropogenic inputs of charred plant material (Supplementary Fig. 9), and lithic artefact analysis. Like layer X (ref. 17), layer 8 has the highest lithic density (Supplementary Tables 2 and 3) of the basal stratigraphic sequence below the Upper Palaeolithic (layer 6-black/dark spotted) and represents the main occupation of the LRJ. Although we did not recover any diagnostic points, two of the artefacts from our excavations are fragmented blades (Fig. 1c, d), which are typical blanks for the LRJ blade points. Similar to the LRJ assemblage from layer X (ref. 17), most of the artefacts from layers 9 and 8 were made of Baltic flint (Supplementary Table 3). This shows a connection of the Ranis LRJ to the lowlands north of the site where the flint was procured. Three small flakes coming from surface shaping and edge retouch are made of quartzite (Fig. 1e). This raw material also occurs in a few artefacts from the 1932–1938 excavation (Supplementary Table 1). Among them is a fragment of a bifacial tool, possibly a leaf point. Except for one chunk, layer 7 contained no artefacts, but a few flint chips were found during sorting of screened excavated sediment from the layer contact 8/7 (Supplementary Table 3). We assign these artefacts to the archaeological horizon of layers 9–8. In contrast to the LRJ layers, flint artefacts are absent in the underlying layers 10 and 11. A similar

low-frequency usage of flint has also been reported for layer XI of the 1932–1938 excavation¹⁷.

We constructed a chronological model based on 28 radiocarbon dates from newly excavated material from layers 11–7, including directly dated human remains, anthropogenically modified bones and charcoal. Bone collagen preservation was exceptional with an average yield of 11.8% (range: 5.3–16.3%, $n = 33$; Supplementary Table 13). Only one date in the model was identified as an outlier, highlighting the stratigraphic integrity of the layers. At the base, layer 11, containing undiagnostic artefacts, dates to 55,860–48,710 cal BP. Layers 9 and 8, associated with the LRJ, date to 47,500–45,770 cal BP and 46,820–43,260 cal BP, respectively (modelled ranges at 95.4% probability; Extended Data Fig. 3 and Supplementary Table 15). The overlying layer 7 dates to 45,890–39,110 cal BP and is sealed by the roof collapse. In addition, six newly identified human bones from layer X in the 1930s collection, thought to be associated with the LRJ, were directly radiocarbon dated (see below). These dates (46,950–42,200 cal BP at 95.4% probability) fit within the range of dates obtained in our model for layers 9 and 8 (Fig. 2 and Extended Data Fig. 3), thus providing additional support for linking the LRJ of layer X (1930s) with our layers 9 and 8.

We carried out a combination of two proteomic screening approaches (matrix-assisted laser desorption ionization–time-of-flight mass spectrometry and liquid chromatography–tandem mass spectrometry) and morphological identification on bone specimens from the 2016–2022 and 1932–1938 excavations (Methods). We were able to retrieve 13 hominin bone specimens in total (Extended Data Table 1). Out of those, four hominin bones were discovered through proteomic methods and derived from the 2016–2022 excavation: one from layer 9 (specimen ID: 16/116-159416) and three from layer 8 (specimen IDs: 16/116-159253, 16/116-159327 and 16/116-159199; Fig. 1a). Among material from the 1932–1938 excavation, we identified nine additional hominin bone specimens, four through proteomic analysis, all from layer X (specimen IDs: R10318, R10355, R10396 and R10400), and five through morphological analysis from boxes labelled with layer X, layers IX and X, or layers X and XI (specimen IDs: R10873, R10874, R10875, R10876 and R10879; Fig. 1a and Supplementary Table 5). The boxes with mixed layer tags from the 1932–1938 excavation are a result of the expedited excavation methods from the 1930s. The hominin remains were in most cases, however, excavated on the same day or within a day of the discovery of LRJ artefacts in the same squares (Extended Data Fig. 2).

To support the identification of endogenous proteomes in all proteomically identified hominin specimens, we evaluated the amino acid degradation and their coverage per identified position. Proteomic deamidation measurements (matrix-assisted laser desorption ionization–time-of-flight and liquid chromatography with tandem mass spectrometry) of the fauna revealed diagenesis of collagen type I consistent with all of the hominin remains (Extended Data Fig. 4 and Supplementary Fig. 10). Finally, we compared our results with the existing reference proteome of Homininae¹⁹ and calculated the proteomic coverage per amino acid position for all of the identified hominin specimens (Extended Data Fig. 5). Our proteomic sequencing results showed that amino acid positions recovered for all hominin specimens analysed with the species by proteome investigation pipeline¹⁹ matched with the Homininae reference proteome. However, owing to limitations in the existing proteomic reference database¹⁹, further taxonomic distinctions among hominin populations are not made.

We tested 11 of the hominin remains for the preservation of ancient mitochondrial DNA (mtDNA). Between 4,413 and 175,688 unique reads mapping to the human mtDNA reference genome were recovered per skeletal fragment. These mtDNA reads had elevated frequencies of cytosine (C)-to-thymine (T) substitutions (32.6% to 49.6% on the 5' end and 19.0% to 47.9% on the 3' end, respectively; Supplementary

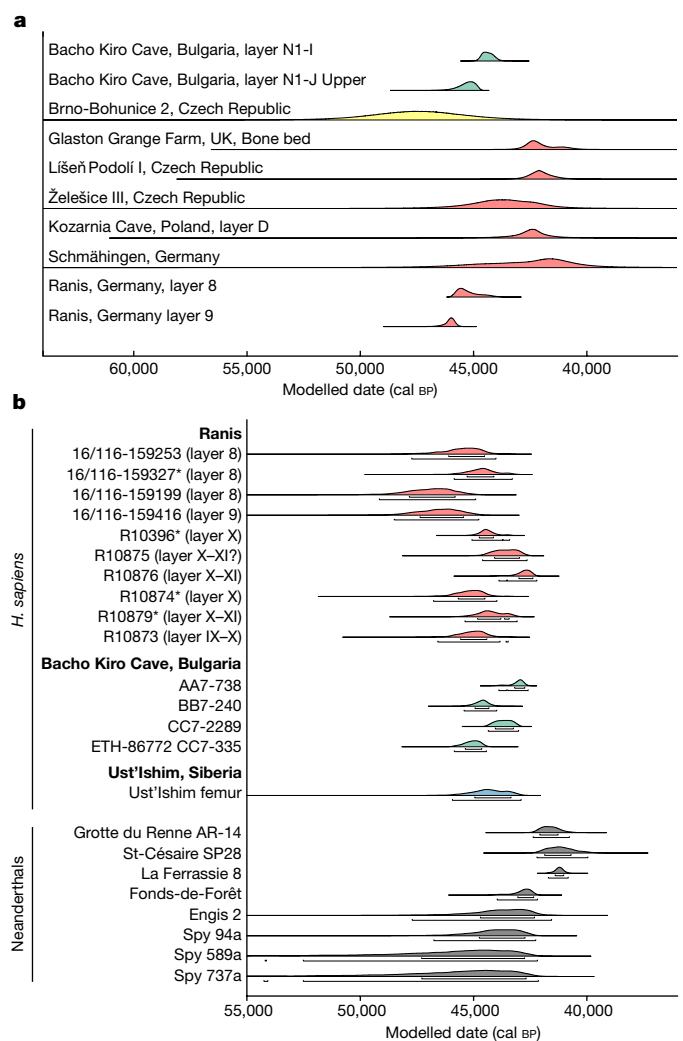


Fig. 2 | Chronological comparison of Ranis with selected contemporary sites and directly dated human remains. **a**, Distributions showing kernel density estimates⁴¹ of radiocarbon dates from LRJ contexts across Europe (red), IUP contexts at Bacho Kiro Cave (green) and TL dates from Brno-Bohunice (yellow). The location of the sites is shown in Supplementary Fig. 1. **b**, Calibrated ranges of directly radiocarbon dated *H. sapiens* from Ranis (LRJ, red), Bacho Kiro Cave (IUP, green) and Ust'-Ishim (no associated archaeology, blue), and Neanderthals (grey) from southwestern France and Belgium. The asterisk marks the Ranis bones for which mtDNA indicates that they originate either from the same or maternally related individuals. The four dates are statistically identical. R10355 and R10318 were not directly dated owing to contamination from conservative treatments (Supplementary Information section 4.1). Layer numbers of the bones from the 1932–1938 excavation (IX, X and XI) refer to labels of boxes in which the finds are stored, which contain material from one or more layers. Data included are shown in Supplementary Tables 17 and 26.

Figs. 14–24), which are indicative of ancient DNA. Positions shown to be informative for differentiating between *H. sapiens*, Neanderthal and Denisovan mtDNA genomes enabled us to identify each of the 11 skeletal fragments as belonging to ancient *H. sapiens* (Supplementary Table 18). Libraries from ten of the eleven skeletal fragments contained sufficient data for reconstructing near-complete mtDNA genomes. Five of these mtDNA genomes showed no pairwise differences among them for the positions covered, suggesting that they stemmed from either the same individual or maternally related individuals (Supplementary Fig. 25 and Supplementary Table 19). Four of these skeletal fragments come from the 1932–1938 collection and one from the 2016–2022

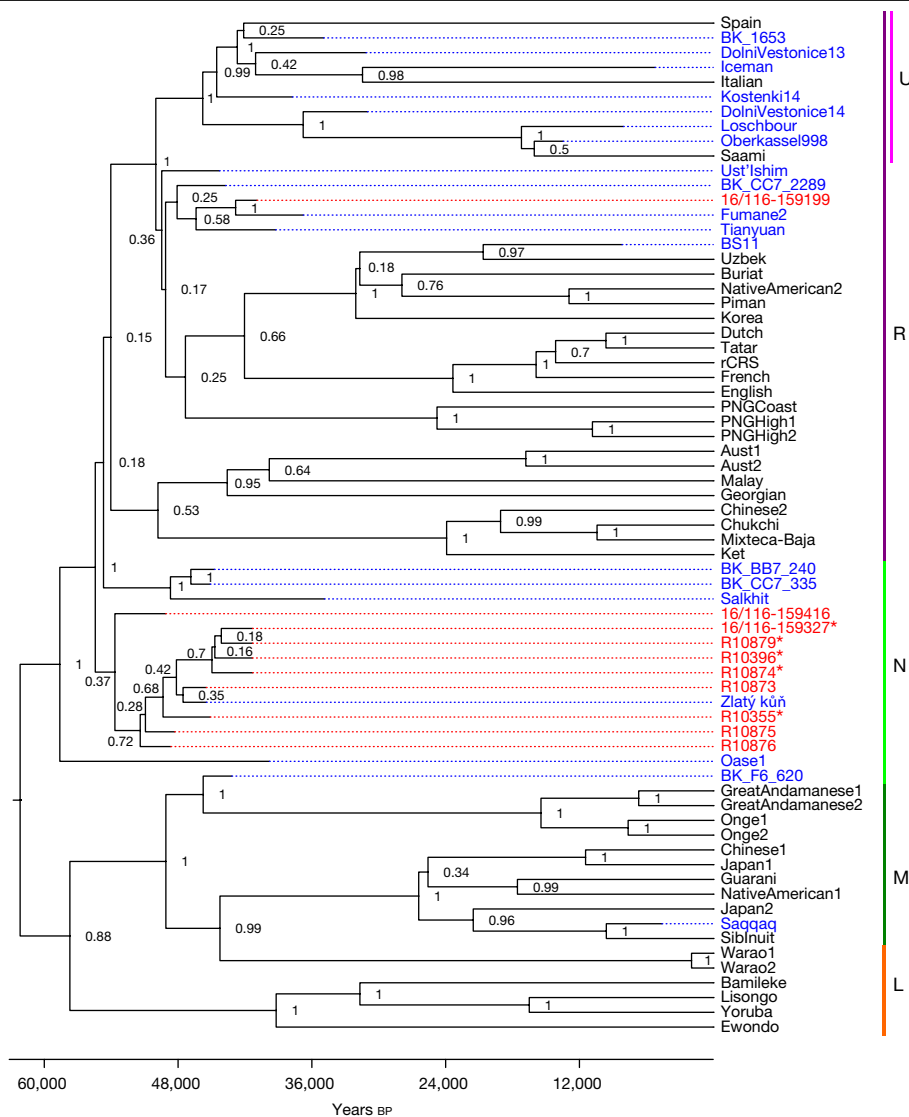


Fig. 3 | Bayesian phylogenetic tree of the newly reconstructed mtDNA genomes with previously published ancient and recent modern human mtDNA genomes constructed with BEAST2. The posterior probability is shown for each branch point and the x axis shows the years before present. Individual genomes are coloured to denote whether they are ancient (blue) or

modern (black) genomes; newly sequenced mtDNA genomes from this study are coloured in red. The Neanderthal mtDNA genomes used to root the tree and modern human mtDNA genomes falling outside the clades shown are not depicted. Asterisks mark mtDNA genomes with no pairwise differences. MtDNA haplogroups (L, M, N, R and U) are labelled in the right column.

excavation (16/116-159327; Fig. 1), providing additional support to the correlation of layers 9 and 8 with layer X. Four of these fragments (16/116-159327 from the 2016–2022 excavation; R10874, R10879 and R10396 from the 1930s collection) also produced statistically indistinguishable radiocarbon dates (Fig. 2). The morphology and stable isotopic values²⁰ of R10874 suggest that it originates from a different individual, consistent with a maternal relation. Notably, whereas nine of the ten reconstructed mtDNA genomes belonged to haplogroup N, one (16/116-159199) was identified as belonging to haplogroup R. When placed onto a phylogenetic tree with other ancient humans, the mtDNA genomes with an N haplogroup cluster together with the mtDNA genome of Zlatý kůň, an individual from the Czech Republic, whose chronological age is around 45,000 years before present on the basis of genetic estimates³ (Fig. 3 and Supplementary Figs. 26 and 27). The estimated mean genetic dates of the Ranis mtDNA genomes ranged from 49,105 to 40,918 years before present (Supplementary Table 22 and Supplementary Fig. 26), consistent with the radiocarbon dates from layers 9 and 8.

The hominin remains from the 2016–2022 and 1932–1938 excavations are associated with a range of animal taxa (Supplementary Table 9). Overall, both zooarchaeological and proteomic analyses identified a total of 17 taxa with a predominance of reindeer (*Rangifer tarandus*). Other taxa included Bovinae (*Bos primigenius* and *Bison priscus*), Cervidae (*Cervus elaphus*), horse (*Equus ferus*) and megafauna (*Coelodonta antiquitatis* and *Mammuthus primigenius*). A variety of carnivores were also identified, dominated by cave bear (*Ursus spelaeus*; Supplementary Table 9). This species composition is consistent with the faunal record of central Europe during Marine Isotope Stage 3 (refs. 21–24). Our analyses suggest that large carnivores accumulated most bone remains with only occasional, short-term site use by human groups (Supplementary Tables 10–12), which is consistent with the recovered ancient sediment DNA and the relatively low lithic counts (Supplementary Tables 1–3) in these LRJ layers²⁰. This is similar to what has been observed at other LRJ sites²⁵. Our sedimentological analyses indicate a temperature decline from layer 9 towards colder climatic conditions in layer 7 (Supplementary Table 4). This agrees with stable

isotope analyses of equid teeth that indicate a temperature decline with low temperatures and an open steppe environment during all phases of the LRJ occupations. Temperatures reconstructed for the coldest phase, about 45,000–43,000 cal BP (overlapping with both layer 8 and layer 7), were 7–15 °C lower than those of the modern day and are consistent with a highly seasonal subarctic climate in full stadial conditions²⁶. On the basis of comparisons with the timing of Greenland stadials and Greenland interstadials in both the North Greenland Ice Core Project and terrestrial sequences in western Germany, the LRJ occupations overlap with a variety of climatic phases including Greenland Stadial 13 (GS13), Greenland Interstadial 12 and GS12, and a temperature decline towards full stadial conditions during the coldest phase is congruent with an interstadial–stadial transition culminating in a pronounced cold phase such as GS12 or GS13 (Extended Data Fig. 3).

In summary, our work shows that the LRJ at Ranis was made by hominins with *H. sapiens* mtDNA. This indicates that pioneer groups of *H. sapiens* expanded rapidly into the higher mid-latitudes, possibly as far as the modern day British Isles (Fig. 1b), before much later expansions into southwestern Europe, where directly dated Neanderthal remains are documented until about 42,000 cal BP (Fig. 2). Although non-directly dated and non-genetically identified, a human deciduous tooth from Grotte Mandrin²⁷ also suggests an *H. sapiens* incursion into southeastern France as early as about 54,000 cal BP. If confirmed, this evidence would create a complex mosaic picture of Neanderthal and *H. sapiens* groups in Europe between about 55,000 and 45,000 cal BP. On the basis of the archaeological and zooarchaeological evidence, the pioneer *H. sapiens* groups were small and possibly left no notable genetic traces in the later Upper Palaeolithic hunter-gatherers in Europe²⁸. The early presence of *H. sapiens* in the modern day British Isles is further evidenced by the disputed dating of the Kent's Cavern maxilla^{7,8,29,30}, probably associated with LRJ stone tools at this site. Archaeological and mtDNA data further suggest that LRJ *H. sapiens* at Ranis were connected to populations of eastern and central Europe. The relationship between the bifacial-point-rich LRJ at Ranis and other chronologically overlapping bifacial point industries of central Europe, such as the Szeletian^{31,32} and Altmühlian^{33,34} (Supplementary Fig. 1b), remains to be explored. If the Initial Upper Palaeolithic (IUP) Bohunician³⁵ of Moravia and the LRJ are related technocomplexes³⁶, then the LRJ is part of the IUP expansion into Europe. There are no human remains preserved from the Bohunician, but the Zlatý kůň *H. sapiens* skull from the Czech Republic overlaps with the dates for both the Bohunician^{35,37} and the LRJ at Ranis. Notably, nine out of ten Ranis mtDNA genomes cluster with the Zlatý kůň individual and one clusters with the Fumane 2 individual, both of whom are other early *H. sapiens* individuals who lived around the same time in Europe as the Ranis specimens described here. This connects the LRJ hominins to a wider population network of initial *H. sapiens* incursions into Europe. Finally, the demonstration that the LRJ was produced by *H. sapiens* fills an important gap in the record of the last Neanderthals and *H. sapiens* in northwestern and central Europe around 45,000 cal BP. The hypothesis that Neanderthals disappeared from northwestern Europe well before the arrival of *H. sapiens*—which is largely based on the chronological hiatus observed between Neanderthal-made late Middle Palaeolithic assemblages and *H. sapiens*-made Aurignacian assemblages³⁸—can now be rejected.

Online content

Any methods, additional references, Nature Portfolio reporting summaries, source data, extended data, supplementary information, acknowledgements, peer review information; details of author contributions and competing interests; and statements of data and code availability are available at <https://doi.org/10.1038/s41586-023-06923-7>.

- Hublin, J.-J. et al. Initial Upper Palaeolithic *Homo sapiens* from Bacho Kiro Cave, Bulgaria. *Nature* **581**, 299–302 (2020).
- Hajdinjak, M. et al. Initial Upper Palaeolithic humans in Europe had recent Neanderthal ancestry. *Nature* **592**, 253–257 (2021).
- Prüfer, K. et al. A genome sequence from a modern human skull over 45,000 years old from Zlatý kůň in Czechia. *Nat. Ecol. Evol.* **5**, 820–825 (2021).
- Jöris, O., Neruda, P., Wiśniewski, A. & Weiss, M. The Late and Final Middle Palaeolithic of central Europe and its contributions to the formation of the regional Upper Palaeolithic: a review and a synthesis. *J. Paleolit. Archaeol.* **5**, 17 (2022).
- Flas, D. The Middle to Upper Paleolithic transition in Northern Europe: the Lincombian-Ranisian-Jerzmanowician and the issue of acculturation of the last Neanderthals. *World Archaeol.* **43**, 605–627 (2011).
- Semal, P. et al. New data on the late Neanderthals: direct dating of the Belgian Spy fossils. *Am. J. Phys. Anthropol.* **138**, 421–428 (2009).
- Higham, T. et al. The earliest evidence for anatomically modern humans in northwestern Europe. *Nature* **479**, 521–524 (2011).
- White, M. & Pettitt, P. Ancient digs and modern myths: the age and context of the Kent's Cavern 4 maxilla and the earliest *Homo sapiens* specimens in Europe. *Eur. J. Archaeol.* **15**, 392–420 (2012).
- Desbrosse, R. & Kozłowski, J. K. *Hommes et Climats à l'Âge du Mammouth: le Paléolithique Supérieur d'Eurasie Centrale* (Masson, 1988).
- Flas, D. La transition du Paléolithique moyen au supérieur dans la plaine septentrionale de l'Europe. *Anthropol. Præhist.* **119**, 1–254 (2008).
- Swainston, S. in *Dorothy Garrod and the Progress of the Palaeolithic: Studies in the Prehistoric Archaeology of the Near East and Europe* (eds Davies, W. & Charles, R.) 41–56 (Oxbow, 1999).
- Jacobi, R., Debenham, N. & Catt, J. A collection of Early Upper Palaeolithic artefacts from Beedings, near Pulborough, West Sussex, and the context of similar finds from the British Isles. *Proc. Prehist. Soc.* **73**, 229–326 (2007).
- Cooper, L. P. et al. An Early Upper Palaeolithic open-air station and Mid-Devensian hyaena den at Grange Farm, Glaston, Rutland, UK. *Proc. Prehist. Soc.* **78**, 73–93 (2012).
- Higham, T. et al. Testing models for the beginnings of the Aurignacian and the advent of figurative art and music: the radiocarbon chronology of Geißenklösterle. *J. Hum. Evol.* **62**, 664–676 (2012).
- Nigst, P. R. et al. Early modern human settlement of Europe north of the Alps occurred 43,500 years ago in a cold steppe-type environment. *Proc. Natl Acad. Sci. USA* **111**, 14394–14399 (2014).
- Djakovic, I., Key, A. & Soressi, M. Optimal linear estimation models predict 1400–2900 years of overlap between *Homo sapiens* and Neanderthals prior to their disappearance from France and northern Spain. *Sci. Rep.* **12**, 15000 (2022).
- Hülle, W. *Die Ilsehöhle unter Burg Ranis, Thüringen: eine Paläolithische Jägerstation* (Gustav Fischer, 1977).
- Grünberg, J. M. New AMS dates for Palaeolithic and Mesolithic camp sites and single finds in Saxony-Anhalt and Thuringia (Germany). *Proc. Prehist. Soc.* **72**, 95–112 (2006).
- Rüther, P. L. et al. SPIN enables high throughput species identification of archaeological bone by proteomics. *Nat. Commun.* **13**, 2458 (2022).
- Smith, G. M. et al. The ecology, subsistence and diet of ~45,000-year-old *Homo sapiens* at Ilsehöhle in Ranis, Germany. *Nat. Ecol. Evol.* <https://doi.org/10.1038/s41559-023-02303-6> (2024).
- Guérin, C. Première biozonation du Pléistocène Européen, principal résultat biostratigraphique de l'étude des Rhinocerotidae (Mammalia, Perissodactyla) du Miocène terminal au Pléistocène supérieur d'Europe Occidentale. *Geobios* **15**, 593–598 (1982).
- Smith, G. M. et al. Subsistence behavior during the Initial Upper Paleolithic in Europe: site use, dietary practice, and carnivore exploitation at Bacho Kiro Cave (Bulgaria). *J. Hum. Evol.* **161**, 103074 (2021).
- Berto, C. et al. Environment changes during Middle to Upper Palaeolithic transition in southern Poland (Central Europe). A multiproxy approach for the MIS 3 sequence of Koziarnia Cave (Kraków-Częstochowa Upland). *J. Archaeol. Sci. Rep.* **35**, 102723 (2021).
- Kahlke, R.-D. *The History of the Origin, Evolution and Dispersal of the Late Pleistocene Mammuthus-Coelodonta Faunal Complex in Eurasia (Large Mammals)* (Mammoth Site of Hot Springs, 1999).
- Hussain, S. T., Weiss, M. & Kellberg Nielsen, T. Being-with other predators: cultural negotiations of Neanderthal-carnivore relationships in Late Pleistocene Europe. *J. Anthropol. Archaeol.* **66**, 101409 (2022).
- Pederzani, S. et al. Stable isotopes show *Homo sapiens* dispersed into cold steppes ~45,000 years ago at Ilsehöhle in Ranis, Germany. *Nat. Ecol. Evol.* <https://doi.org/10.1038/s41559-023-02318-z> (2024).
- Slimak, L. et al. Modern human incursion into Neanderthal territories 54,000 years ago at Mandrin, France. *Sci. Adv.* **8**, eabj9496 (2022).
- Posth, C. et al. Palaeogenomics of Upper Palaeolithic to Neolithic European hunter-gatherers. *Nature* **615**, 117–126 (2023).
- Hedges, R. E. M., Housley, R. A., Law, I. A. & Bronk, C. R. Radiocarbon dates from the Oxford AMS system: archaeometry datelist 9. *Archaeometry* **31**, 207–234 (1989).
- Proctor, C., Douka, K., Proctor, J. W. & Higham, T. The age and context of the KC4 maxilla, Kent's Cavern, UK. *Eur. J. Archaeol.* **20**, 74–97 (2017).
- Mester, Z. What about the Szeletian leaf point as *fossile directeur*?. *Študijné Zvesti Archeologického Ústavu SAV Suppl.* **2**, 49–62 (2021).
- Prošek, F. Szeletien na Slovensku. *Slov. Archeol.* **1**, 133–194 (1953).
- Bohmers, A. Die Höhlen von Mauern. Teil I. Kulturgeschichte der Altsteinzeitlichen Besiedlung. *Palaeohistoria* **1**, 3–58 (1951).
- Bosinski, G. *Die Mittelpaläolithischen Funde im Westlichen Mitteleuropa* (Böhlau, 1967).
- Richter, D., Tostevin, G. & Škrdl, P. Bohunician technology and thermoluminescence dating of the type locality of Brno-Bohunice (Czech Republic). *J. Hum. Evol.* **55**, 871–885 (2008).
- Demidenko, Y. E. & Škrdl, P. Lincombian-Ranisian-Jerzmanowician industry and South Moravian sites: a *Homo sapiens* Late Initial Upper Paleolithic with Bohunician industrial generic roots in Europe. *J. Paleolit. Archaeol.* **6**, 17 (2023).

37. Škrdla, P. Middle to Upper Paleolithic transition in Moravia: new sites, new dates, new ideas. *Quat. Int.* **450**, 116–125 (2017).
38. Devières, T. et al. Reevaluating the timing of Neanderthal disappearance in Northwest Europe. *Proc. Natl Acad. Sci. USA* **118**, e2022466118 (2021).
39. QGIS Development Team. *QGIS Geographic Information System*. <http://qgis.osgeo.org>. (Open Source Geospatial Foundation Project, 2023).
40. Reuter, H. I., Nelson, A. & Jarvis, A. An evaluation of void-filling interpolation methods for SRTM data. *Int. J. Geogr. Inf. Sci.* **21**, 983–1008 (2007).
41. Bronk-Ramsey, B. C. Methods for summarizing radiocarbon datasets. *Radiocarbon* **59**, 1809–1833 (2017).

Publisher's note Springer Nature remains neutral with regard to jurisdictional claims in published maps and institutional affiliations.



Open Access This article is licensed under a Creative Commons Attribution 4.0 International License, which permits use, sharing, adaptation, distribution and reproduction in any medium or format, as long as you give appropriate credit to the original author(s) and the source, provide a link to the Creative Commons licence, and indicate if changes were made. The images or other third party material in this article are included in the article's Creative Commons licence, unless indicated otherwise in a credit line to the material. If material is not included in the article's Creative Commons licence and your intended use is not permitted by statutory regulation or exceeds the permitted use, you will need to obtain permission directly from the copyright holder. To view a copy of this licence, visit <http://creativecommons.org/licenses/by/4.0/>.

© The Author(s) 2024

Methods

Excavation methods

We located and reopened 18 squares on the grid line of the main east–west trench from 1934 and excavated an 8-m-deep sequence of 12 adjacent squares (Extended Data Fig. 1b and Supplementary Figs. 2b and 3–8). Layers were identified using lithological as well as archaeological criteria, if available. Stratigraphic units were subsequently numbered from top to bottom, independently of the 1932–1938 excavation¹⁷. The lower layers, from layer 6 to bedrock, were excavated over 2.25 m². Large rocks within the sequence (that is, collapsed parts of the former cave roof) prevented us from enlarging the excavation. To access the deeper stratigraphy that includes the transition period of layers 9 and 8 (Hülle: X), we removed a 1.7-m-thick rock (Extended Data Fig. 1c and Supplementary Figs. 6 and 8) that separated these layers from the overlying Upper Palaeolithic layer 6-black/dark spotted (Hülle: VIII)¹⁷. The same rock extended into squares 35 and 37 from the Hülle excavation¹⁷. Hülle did not remove this rock and never excavated below it. We therefore incorporated these two squares below the rock into our excavation (1003/1000 and half of 1004/1000; Extended Data Fig. 1b). Although rock removal required substantial efforts, the rock-fall provided an ideal situation for the underlying sequence, as it was sealed from post-depositional disturbances by geological processes, humans and animals.

Owing to the depth of the sequence, we secured the walls with wooden planks and metal poles during the progress of the excavation. This work was carried out professionally (by a construction firm) and inspected. Before the walls were closed and secured, all profiles were documented (see below).

We excavated using current standards for Palaeolithic sites. We established an arbitrary excavation grid oriented along the former east–west trench of the 1932–1938 excavation, which was later georeferenced in the global Universal Transverse Mercator coordinate system. We removed sediments in 10-l buckets separated by layer. We recorded the location of each bucket with two sets of three-dimensional (3D) coordinates, one at the beginning and one at the end of each bucket. The sediments were then wet-screened through 4-mm and 2-mm meshes. Single finds >20 mm (lithics and fauna) and samples (sediment and micromorphology) were assigned unique IDs; their layer, date of excavation and excavator were recorded, and 3D coordinates were measured using a Leica total station (5" accuracy). The total station measurement and attribute recording were carried out with EDM-mobile, a self-authored software. At the end of each day, we transferred these data to the primary database for the project. Objects with an identifiable long axis were measured with two coordinates at their endpoints to record bearing and plunge. Stones >10 mm were measured with one coordinate at the base and stones >20 mm were recorded with six coordinates (representing the three axes of the object) to document volume and orientation. Large rocks were documented using multiple measurements.

We documented layers, special features and profiles in highly detailed and precise 3D models using structure from motion (Agisoft Metashape), total station measurements, digital photographs and drawings. The 3D models were georeferenced with control points recorded with the total station to align to the excavation grid.

Proteomic screening

We proteomically screened 1,322 morphologically unidentified fragmentary bone specimens from layers 7–12 (2016–2022 excavation) and layers IX–XI (1932–1938 excavation) with zooarchaeology by mass spectrometry (ZooMS)⁴² and a subset of 341 bone specimens with the species by proteome investigation (SPIN) workflow¹⁹. Generally, we targeted specimens >2 cm in length to enable future direct radiocarbon dating and ancient DNA analysis. We measured bone length for most specimens, and recorded anthropogenic, carnivore and taphonomic

modifications for all of them. Sampling was carried out using pliers or a dental drill. Negative controls were also included in the study (Supplementary Table 6).

First, all specimens were analysed through ZooMS analysis. A total of 769 specimens were derived from the 1932–1938 excavation (Supplementary Table 24), and 553 specimens derived from the 2016–2022 excavation (Supplementary Table 23). Extraction and analytical protocols followed in ZooMS were previously published⁴³. In brief, a small piece of bone (about 5 mg) from each specimen was suspended and denatured in 50 mM ammonium bicarbonate pH 8.0 for 1 h at 65 °C. The samples were digested overnight at 37 °C with 50 mM trypsin solution, acidified using 5% trifluoroacetic acid (TFA) and purified using a HyperSep C18 filter plate (Thermo Scientific). Matrix-assisted laser desorption ionization–time-of-flight MS (MALDI–TOF MS) analysis for the first 649 specimens was conducted at the IZI Fraunhofer in Leipzig, Germany, in an autoflex speed LRF MALDI–TOF (Bruker) with reflector mode, positive polarity and spectra collected in the mass-to-charge range 1,000–3,500 *m/z*. The remaining specimens were analysed on a MALDI–TOF 5800AB Sciex instrument at the Ecole Supérieure de Physique et Chimie Industrielle, Paris, France, in positive reflector mode, covering a mass-to-charge range of 1,000 to 3,500 Da. MALDI–TOF MS replicates (*n* = 3) were averaged for each sample and manually inspected for the presence of relevant peptide markers (A–G)⁴⁴ in mMass v5.5.0 (ref. 45). MALDI–TOF MS spectra were analysed in comparison to a reference database containing collagen-peptide marker masses of all medium- to larger-sized genera in existence in western Eurasia during the late Pleistocene^{42,46,47}. Glutamine deamidation values were calculated using the Betacalc3 package⁴⁸ on the basis of COL1 α 1 508–519 deamidation.

Second, we proteomically sequenced a subset of 341 fragmentary bone specimens, previously identified by ZooMS, with SPIN¹⁹. A total of 129 specimens were retrieved during the 1932–1938 excavation and 212 specimens came from the 2016–2022 excavation (Supplementary Table 7). Approximately 5 mg of each bone specimen was suspended and demineralized overnight in 5% hydrochloric acid (HCl) and a 0.1% nonyl phenoxypolyethoxylethanol (NP-40) solution at room temperature with continuous shaking. Reduction, alkylation and collagen gelatinization were facilitated by adding 0.1 M tris(2-carboxyethyl) phosphine (TCEP) and 0.2 M *N*-ethylmaleimide (NEM) at 60 °C, for 1 h. The protein aggregation capture and digestion took place on a KingFisher Flex (ThermoFisher Scientific) magnetic bead-handling robot. Protein extracts were mixed with magnetic SiMAG-Sulfon beads. Protein aggregation was initiated with the addition of 70% acetonitrile (ACN). The beads and the proteins were washed in 70% acetonitrile, 80% ethanol and 100% acetonitrile consecutively. Then, proteins were released into a solution of 20 mM Tris pH 8.5, 1 μ g ml⁻¹ LysC and 2 μ g ml⁻¹ trypsin for proteome digestion. The digestion was finalized outside the robot at 37 °C, overnight. The peptides were acidified with 5% trifluoroacetic acid and purified in a C18 Evotip. The specimens were analysed on an Evosep One (Evosep)⁴⁹ connected in line to an Orbitrap Exploris tandem mass spectrometer (ThermoFisher) at the Centre for Protein Research at the University of Copenhagen, Denmark. The samples were analysed with the 200SPD Evosep One method on a short online liquid chromatography gradient in MS/MS data-independent acquisition (DIA) mode using a homemade 3- μ m silica column. Full scans ranged from 350 to 1,400 *m/z* and were measured at 120,000 resolution, 45 ms maximum IT, 300% AGC target. Precursors were selected for data-independent fragmentation in 15 windows ranging from 349.5 to 770.5 *m/z* and 3 windows ranging from 769.5 to 977.5 *m/z*, with 1-*m/z* overlap.

DIA MS/MS spectra were loaded into Biognosys Spectronaut^{50,51} v15.6.211220, and analysed using either library-based (libDIA) or library-free DirectDIA (dirDIA) search. The required peptide identification data were generated with a Spectronaut report based on the SPIN.rs¹⁹ scheme for DIA analysis, and the library-based and the library-free

Article

DirectDIA searches were carried out as described in previous studies¹⁹. The utilized protein sequence databases contained entries for the 20 most common bone proteins from a wide range of species represented in UniProt and Genbank. The species determination was carried out in R v4.1.2 (ref. 52) as described previously¹⁹. Variable modifications included in the search were oxidation (methionine), deamidation (asparagine-N, glutamine-Q), glutamine to pyroglutamic acid, glutamate to pyroglutamate and proline hydroxylation, while NEM derivatization of cysteine was included as a fixed modification. In part, SPIN taxonomic identification was based on gene-wise alignment of protein entries in the searched database and the computation of two quality control markers for estimating the confidence of each taxonomic assignment. As a result, we noted that the SPIN¹⁹ and ZooMS taxonomic reference databases were composed of partly overlapping but highly different taxonomic entities (Supplementary Table 8), with absences of some taxonomic groups in SPIN resulting in false species assignments despite high-confidence bone proteome data (Supplementary Figs. 11 and 12). The six Ranis specimens subjected to liquid chromatography–MS/MS with data-dependent acquisition were analysed as described previously⁵³.

Morphological identification of hominin remains

All of the faunal remains from the 1932–1938 excavation housed at the Landesamt für Denkmalpflege und Archäologie Sachsen-Anhalt in Halle (Saale) were sorted to potentially identify human remains among them. This consisted of examining each skeletal element of any size and visually assessing characteristics such as overall shape, size, tissue proportions, developmental stage and presence of particular anatomical features to discern the right category for a bone or tooth. Several potentially hominin specimens were isolated in this manner. They come mostly from the upper layers of the site. The human status of those from the lower layers was confirmed through DNA analysis, and they were subsequently directly radiocarbon dated.

Radiocarbon dating

Radiocarbon dating of 30 samples from layers 11–7 of the 2016–2022 excavation was undertaken to establish a site chronology, including 27 bone specimens and 3 charcoal samples (Supplementary Table 13). The bone specimens included 4 hominin bones and 23 faunal bones (14 of which showed signs of anthropogenic modification including butchery, cut marks and percussion notches). Six hominin bones from the 1930s collections were radiocarbon dated to determine their chronological position in relation to the new site chronology. Two additional hominin bones from the 1930s collection had been conserved with paraffin so they were excluded from dating owing to the risk of contamination (Supplementary Fig. 13 and Supplementary Information section 4.1).

Pretreatment of the bone samples was carried out in the Department of Human Evolution at the Max Planck Institute for Evolutionary Anthropology in Leipzig, Germany. Collagen was extracted from the faunal bone samples using about 300–600 mg material following an acid–base–acid plus ultrafiltration protocol published previously^{54,55}, and from the human bones using about 55–160 mg bone material following a previously published protocol for small sample extraction⁵⁴ (Supplementary Information section 4.1). Two faunal bones were pretreated with a second collagen extraction protocol to test for the presence of modern carbon contamination resulting from humic acids (Supplementary Table 14). Suitability for dating was assessed on the basis of the collagen yield (as a percentage of dry bone weight) with a 1% minimum requirement and the elemental values, measured on a ThermoFinnigan Flash elemental analyser coupled to a Thermo Delta plus XP isotope ratio mass spectrometer. To pass the quality threshold, samples were required to fall within the accepted elemental ranges of modern collagen samples (about 35–45% C; about 11–16% N; C/N between 2.9 and 3.6)⁵⁶.

The collagen extracts were graphitized⁵⁷ and dated at the Laboratory for Ion Beam Physics at ETH Zurich, Switzerland on a MICADAS accelerator mass spectrometer (AMS)^{58,59}. Sub-samples of two bones that date beyond the limit of the ¹⁴C method (>50,000 BP) ('background' bones) were pretreated and dated alongside the samples to monitor laboratory-based contamination. The accelerator mass spectrometer measurements of the collagen backgrounds were used in the age correction of each batch of samples in BATS⁶⁰, with an additional 1‰ error added, as per the standard practice (Supplementary Table 13).

The three charcoal samples were pretreated at the Curt-Engelhorn-Center for Archaeometry GmbH (MAMS) using a softened ABOx protocol before being combusted to CO₂ in an elemental analyser, converted catalytically to graphite and measured on a MICADAS accelerator mass spectrometer⁶¹. Two of the three charcoal samples had very low percentages of C following combustion and were therefore excluded from the site chronological modelling.

Measured radiocarbon ages are reported in Supplementary Table 13 with the abbreviation BP, meaning radiocarbon years before AD 1950, and are reported with 1 σ errors, whereas calibrated radiocarbon ranges are denoted as cal BP and are given at the 95.4% (2 σ) probability range. All ages have been rounded to the nearest 10 yr. Calibration and Bayesian modelling of the radiocarbon dates was carried out in OxCal v4.4 (ref. 62) using the IntCal20 calibration curve⁶³. A multi-phase model was constructed for the dates from the 2016–2022 excavation using stratigraphic information as a prior. A 'general' outlier model was used to assess the likelihood of each sample being an outlier with prior probabilities set to 5%. The date ranges for each layer discussed in the text are the output of the site chronological modelling. Further information and the OxCal code is included in Supplementary Information sections 4.2 and 4.3 and Supplementary Tables 15 and 16.

Ancient DNA analysis

Eleven skeletal remains were screened for ancient human DNA preservation. Between 6.1 and 63.9 mg of bone powder was drilled from each specimen in a dedicated clean room at the Max Planck Institute for Evolutionary Anthropology in Leipzig, Germany, or the former Max Planck Institute for the Science of Human History in Jena, Germany. DNA extracts were prepared following the protocol described previously⁶⁴ with buffer 'D' and subsequently converted into single-stranded and double-indexed libraries following the automated protocol described previously⁶⁵. Libraries from 10 of the 11 remains were subsequently enriched for human mtDNA using the singleplex automated capture protocol described earlier⁶⁶. The resulting libraries were sequenced on either the Illumina NextSeq or MiSeq platforms (2 × 76 cycles). No cross-contamination of DNA molecules due to index hopping was detected in these libraries on the basis of calculations from a previously published method⁶⁶. For one of the specimens, R10873, four single-stranded libraries were prepared from the same extract in the Jena facilities following the protocol described above and pooled together. Shotgun sequencing of the pooled libraries was carried out at the SciLifeLab, on a full Novaseq S4-200 flow-cell using 2 × 75-base-pair paired-end sequencing.

Base calling was carried out with Bustard, and reads were overlap merged using leeHom⁶⁷. Mapping was carried out with BWA⁶⁸ using adjustments for ancient DNA (-n 0.01 -o 2 -l 16500)⁶⁹. All libraries were mapped to the human mtDNA revised Cambridge Reference Sequence (NC_01290)⁷⁰. Reads from the libraries generated from the same skeletal fragment were then merged using Samtools merge⁷¹. PCR duplicates, reads shorter than 35 base pairs or with a mapping quality less than 25 were removed using bam-rmdup (v0.6.3; <https://bitbucket.org/ustenzel/biohazard>). Each library was then evaluated for the presence of authentic ancient human DNA (Supplementary Table 25). The proportion of present day human DNA contamination was estimated using AuthentiCT⁷². Support for *H. sapiens*, Neanderthal or Denisovan

mtDNA among the recovered mtDNA fragments was determined using sets of previously published 'diagnostic' positions⁷³ that allow differentiation among these hominin mtDNA types (Supplementary Information section 5).

Full mtDNA genomes were reconstructed for 10 of the 11 specimens with >70-fold coverage of the mtDNA genome. Consensus bases were called using either all fragments (for the libraries with the levels of present day human DNA contamination <5%) or deaminated fragments alone (for the libraries with the levels of present day human DNA contamination >5%), requiring each site to be covered with at least five DNA fragments and 80% support while ignoring the C-to-T substitutions on the first and/or the last seven positions from the alignment ends. The haplogroup of each reconstructed mtDNA genome was determined using HaploGrep2 (v2.4.0)⁷⁴. MAFFT (v7.453)⁷⁵ was used to realign all ten newly reconstructed human mtDNA genomes to the rCRS with previously published mtDNA genomes from 54 modern humans, 19 ancient humans and 2 Neanderthals. A phylogenetic tree relating these mtDNA genomes was generated using BEAST2 v2.6.6 (ref. 76) with a Bayesian skyline tree model and strict clock model (see Supplementary Information section 5 for model and parameter details; Supplementary Table 21). Molecular dates for the new mtDNA genomes were estimated by calibrating the tree with the mtDNA genomes of individuals with direct radiocarbon dates (Supplementary Table 20). To differentiate between calibrated radiocarbon ranges and molecular dates, we use cal BP before present for the former and years before present for the latter.

Reporting summary

Further information on research design is available in the Nature Portfolio Reporting Summary linked to this article.

Data availability

The raw LC-MS/MS proteomics data for the DIA search have been deposited to the ProteomeXchange Consortium through the PRIDE⁷⁷ partner repository under accession code PXD043272. The raw LC-MS/MS and MaxQuant search proteomics data for six bone specimens analysed in DDA mode included in this study have been deposited to the ProteomeXchange Consortium through the PRIDE partner repository with the dataset identifier PXD042321. The MALDI-TOF.mzml and.msdf type files included in this study are available at <https://doi.org/10.5281/zenodo.8063812> (ref. 78). The newly reconstructed mtDNA sequences are available at <https://doi.org/10.5061/dryad.1jwstqk0s> and the sequencing data are available at the European Nucleotide Archive (PRJEB67776).

Code availability

The full code description is provided in the Supplementary Information.

42. Buckley, M., Collins, M., Thomas-Oates, J. & Wilson, J. C. Species identification by analysis of bone collagen using matrix-assisted laser desorption/ionisation time-of-flight mass spectrometry. *Rapid Commun. Mass Spectrom.* **23**, 3843–3854 (2009).
43. van Doorn, N. L., Hollund, H. & Collins, M. J. A novel and non-destructive approach for ZooMS analysis: ammonium bicarbonate buffer extraction. *Archaeol. Anthropol. Sci.* **3**, 281–289 (2011).
44. Brown, S., Douka, K., Collins, M. J. & Richter, K. K. On the standardization of ZooMS nomenclature. *J. Proteomics* **235**, 104041 (2021).
45. Strohal, M., Kavan, D., Novák, P., Volný, M. & Havlíček, V. mMass 3: a cross-platform software environment for precise analysis of mass spectrometric data. *Anal. Chem.* **82**, 4648–4651 (2010).
46. Kirby, D. P., Buckley, M., Promise, E., Trauger, S. A. & Holdcraft, T. R. Identification of collagen-based materials in cultural heritage. *Analyst* **138**, 4849–4858 (2013).
47. Buckley, M. et al. Species identification of archaeological marine mammals using collagen fingerprinting. *J. Archaeol. Sci.* **41**, 631–641 (2014).
48. Wilson, J., van Doorn, N. L. & Collins, M. J. Assessing the extent of bone degradation using glutamine deamidation in collagen. *Anal. Chem.* **84**, 9041–9048 (2012).
49. Bache, N. et al. A novel LC system embeds analytes in pre-formed gradients for rapid, ultra-robust proteomics. *Mol. Cell. Proteomics* **17**, 2284–2296 (2018).
50. Bruderer, R. et al. Optimization of experimental parameters in data-independent mass spectrometry significantly increases depth and reproducibility of results. *Mol. Cell. Proteomics* **16**, 2296–2309 (2017).
51. Bekker-Jensen, D. B. et al. Rapid and site-specific deep phosphoproteome profiling by data-independent acquisition without the need for spectral libraries. *Nat. Commun.* **11**, 787 (2020).
52. R Core Team. *R: A language and Environment for Statistical Computing*. <https://www.R-project.org/> (Foundation for Statistical Computing, 2013).
53. Mylopotamitaki, D. et al. Comparing extraction method efficiency for high-throughput palaeoproteomic bone species identification. *Sci. Rep.* **13**, 18345 (2023).
54. Fewlass, H. et al. Pretreatment and gaseous radiocarbon dating of 40–100 mg archaeological bone. *Sci. Rep.* **9**, 5342 (2019).
55. Talamo, S., Fewlass, H., Maria, R. & Jaouen, K. 'Here we go again': the inspection of collagen extraction protocols for ¹⁴C dating and palaeodietary analysis. *Sci. Technol. Archaeol. Res.* **7**, 62–77 (2021).
56. van Klinken, G. J. Bone collagen quality indicators for palaeodietary and radiocarbon measurements. *J. Archaeol. Sci.* **26**, 687–695 (1999).
57. Wacker, L., Némec, M. & Bourquin, J. A revolutionary graphitisation system: fully automated, compact and simple. *Nucl. Instrum. Methods Phys. Res. B* **268**, 931–934 (2010).
58. Synal, H.-A., Stocker, M. & Suter, M. MICADAS: a new compact radiocarbon AMS system. *Nucl. Instrum. Methods Phys. Res. B* **259**, 7–13 (2007).
59. Wacker, L. et al. MICADAS: routine and high-precision radiocarbon dating. *Radiocarbon* **52**, 252–262 (2010).
60. Wacker, L., Christl, M. & Synal, H.-A. Bats: a new tool for AMS data reduction. *Nucl. Instrum. Methods Phys. Res. B* **268**, 976–979 (2010).
61. Kromer, B., Lindauer, S., Synal, H.-A. & Wacker, L. MAMS – a new AMS facility at the Curt-Engelhorn-Centre for Archaeometry, Mannheim, Germany. *Nucl. Instrum. Methods Phys. Res. B* **294**, 11–13 (2013).
62. Bronk-Ramsey, C. Bayesian analysis of radiocarbon dates. *Radiocarbon* **51**, 337–360 (2009).
63. Reimer, P. J. et al. The IntCal20 Northern Hemisphere radiocarbon age calibration curve (0–55 cal kBP). *Radiocarbon* **62**, 725–757 (2020).
64. Rohland, N., Glocke, I., Aximu-Petri, A. & Meyer, M. Extraction of highly degraded DNA from ancient bones, teeth and sediments for high-throughput sequencing. *Nat. Protoc.* **13**, 2447–2461 (2018).
65. Gansauge, M. T., Aximu-Petri, A., Nagel, S. & Meyer, M. Manual and automated preparation of single-stranded DNA libraries for the sequencing of DNA from ancient biological remains and other sources of highly degraded DNA. *Nat. Protoc.* **15**, 2279–2300 (2020).
66. Zavala, E. I. et al. Quantifying and reducing cross-contamination in single- and multiplex hybridization capture of ancient DNA. *Mol. Ecol. Resour.* **22**, 2196–2207 (2022).
67. Renaud, G., Stenzel, U. & Kelso, J. leeHom: adaptor trimming and merging for Illumina sequencing reads. *Nucleic Acids Res.* **42**, e141 (2014).
68. Li, H. & Durbin, R. Fast and accurate long-read alignment with Burrows-Wheeler transform. *Bioinformatics* **26**, 589–595 (2010).
69. Meyer, M. et al. A high-coverage genome sequence from an archaic Denisovan individual. *Science* **338**, 222–226 (2012).
70. Andrews, R. M. et al. Reanalysis and revision of the Cambridge reference sequence for human mitochondrial DNA. *Nat. Genet.* **23**, 147 (1999).
71. Li, H. et al. The Sequence Alignment/Map format and SAMtools. *Bioinformatics* **25**, 2078–2079 (2009).
72. Peyrégne, S. & Peter, B. M. AuthenticCT: a model of ancient DNA damage to estimate the proportion of present-day DNA contamination. *Genome Biol.* **21**, 246 (2020).
73. Zavala, E. I. et al. Pleistocene sediment DNA reveals hominin and faunal turnovers at Denisova Cave. *Nature* **595**, 399–403 (2021).
74. Weissensteiner, H. et al. HaploGrep 2: mitochondrial haplogroup classification in the era of high-throughput sequencing. *Nucleic Acids Res.* **44**, W58–W63 (2016).
75. Katoh, K. & Standley, D. M. MAFFT multiple sequence alignment software version 7: improvements in performance and usability. *Mol. Biol. Evol.* **30**, 772–780 (2013).
76. Bouckaert, R. et al. BEAST 2.5: an advanced software platform for Bayesian evolutionary analysis. *PLoS Comput. Biol.* **15**, e1006650 (2019).
77. Perez-Riverol, Y. et al. The PRIDE database and related tools and resources in 2019: improving support for quantification data. *Nucleic Acids Res.* **47**, D442–D450 (2019).
78. Chue Hong, N. P. et al. Software Citation Checklist for Authors (0.9.0). *Zenodo*, <https://doi.org/10.5281/zenodo.3479199> (2019).
79. Svensson, A. et al. A 60 000 year Greenland stratigraphic ice core chronology. *Clim. Past* **4**, 47–57 (2008).
80. Rasmussen, S. O. et al. A stratigraphic framework for abrupt climatic changes during the Last Glacial period based on three synchronized Greenland ice-core records: refining and extending the INTIMATE event stratigraphy. *Quat. Sci. Rev.* **106**, 14–28 (2014).
81. Kern, O. A. et al. A near-continuous record of climate and ecosystem variability in Central Europe during the past 130 kys (Marine Isotope Stages 5–1) from Fürmoos, southern Germany. *Quat. Sci. Rev.* **284**, 107505 (2022).
82. Sirocko, F. et al. The ELSA-Vegetation-Stack: reconstruction of landscape evolution zones (LEZ) from laminated Eifel maar sediments of the last 60,000 years. *Glob. Planet. Change* **142**, 108–135 (2016).
83. Myrvoll-Nilsen, E., Riechers, K., Rypdal, M. W. & Boers, N. Comprehensive uncertainty estimation of the timing of Greenland warmings in the Greenland ice core records. *Clim. Past* **18**, 1275–1294 (2022).

Acknowledgements This project received funding from the European Union's Horizon 2020 research and innovation programme under the Marie Skłodowska-Curie grant agreement number 861389 - PUSHH. The radiocarbon dating was financially supported by the Max Planck Society and the Thuringian State Office for the Preservation of Historical Monuments and

Article

Archaeology, Technical assistance in sample pretreatment for radiocarbon dating was provided by M. Trost, L. Klausnitzer and S. Steinbrenner. The excavations and much of the subsequent analysis were financially supported by the Max Planck Society. F.W. has received funding from the European Research Council under the European Union's Horizon 2020 research and innovation programme (grant agreement number 948365). We thank E. Demey for running all of the MALDI analyses at the Ecole Supérieure de Physique et Chimie Industrielle (Paris, France); the IZI Fraunhofer, S. Kalkhof and J. Schmidt for providing access to the MALDI-TOFMS instrument in Leipzig, Germany; P. L. Rütter, Z. Fagernäs and L. Paskulin for assistance on the proteomic analysis; and the Ranis excavation team, especially C. Bock, R. Roa Romero, W.E. Lüdtke, H. Rausch and C. Lechner. E.I.Z. received funding from the Miller Institute for Basic Research in Science, University of California Berkeley. H.F. received funding from the European Molecular Biology Organisation (grant number ALTF 590-2021). G.M.S. is funded by the European Union's Horizon 2020 research and innovation program under the Marie Skłodowska-Curie scheme (grant agreement no. 101027850). Genetics data were partially produced by the Ancient DNA Core Unit of the Max Planck Institute for Evolutionary Anthropology, which is funded by the Max Planck Society. We acknowledge support from the National Genomics Infrastructure in Stockholm funded by Science for Life Laboratory, the Knut and Alice Wallenberg Foundation and the Swedish Research Council, and NAISS for assistance with massively parallel sequencing and access to the UPPMAX computational infrastructure.

Author contributions This study was designed by M.W., T.S. and J.-J.H. Archaeological fieldwork, sampling coordination and contributions were conducted by M.W., T.L., M.S., T.S. and S.P.M. Sample preparations and subsequent analyses were carried out by D.M., M.W., H.F., E.I.Z., H.R., A.P.S., M. Hajdinjak, G.M.S., K.R., V.S.-M., S.P., E.E., F.S.H., H.X., J.H., A.K., T.L., M.S., M. Hein, S.T. and F.W. The original manuscript was prepared by D.M., M.W., H.F., E.I.Z., H.R., S.P., F.W., G.M.S., T.S., S.P.M. and J.-J.H. and reviewed by all co-authors.

Funding Open access funding provided by Max Planck Society.

Competing interests The authors declare no competing interests.

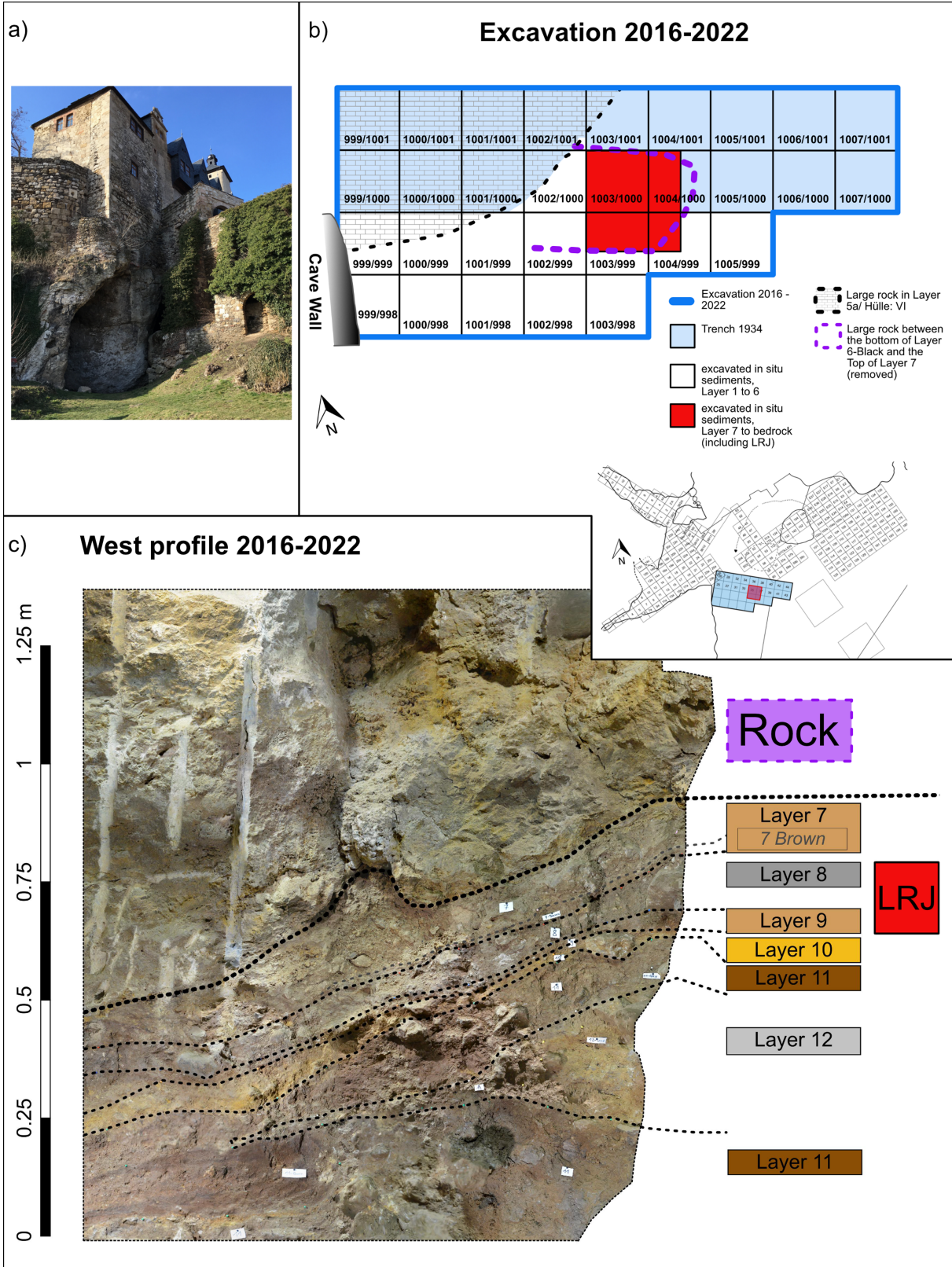
Additional information

Supplementary information The online version contains supplementary material available at <https://doi.org/10.1038/s41586-023-06923-7>.

Correspondence and requests for materials should be addressed to Marcel Weiss or Jean-Jacques Hublin.

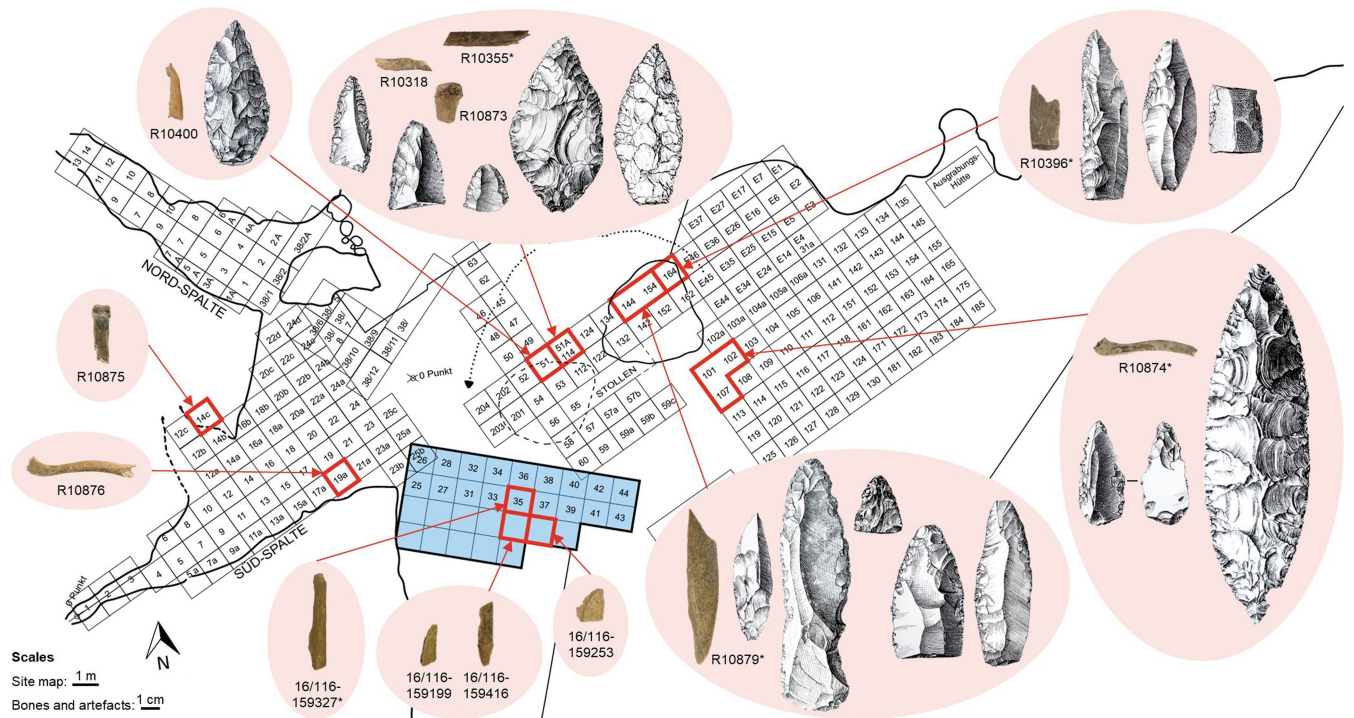
Peer review information *Nature* thanks William Banks, Maarten Blaauw, Olaf Jöris, Nicolas Zwyns and the other, anonymous, reviewer(s) for their contribution to the peer review of this work.

Reprints and permissions information is available at <http://www.nature.com/reprints>.



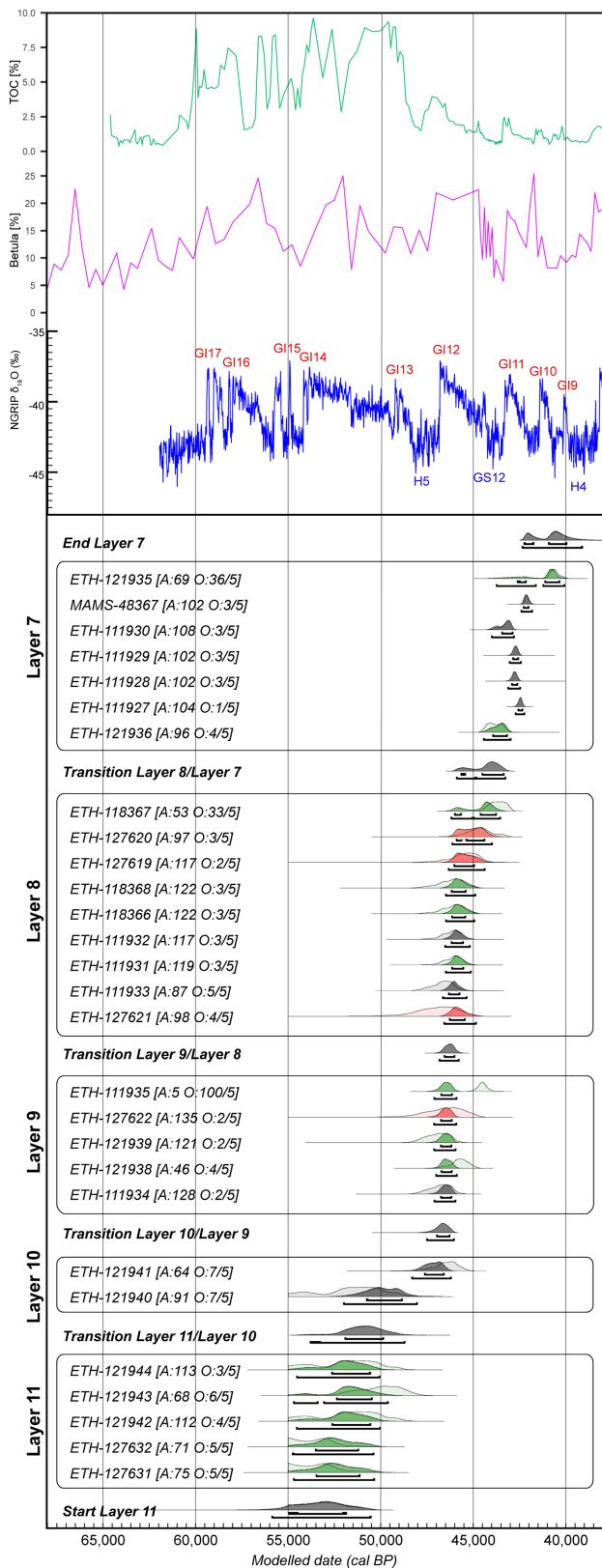
Extended Data Fig. 1 | Ranis site plan and main West profile of the 2016–2022 excavation. a) Ilsenhöhle Ranis. **b)** Plan of the 2016–2022 excavation. The basal sequence including the LRJ layers were excavated in the red area of squares 1003/999, 1003/1000, 1004/999, and 1004/1000. The purple dashed line marks

the removed rock. The inset shows the location of our excavation area relative to the plan of the 1932–1938 excavation¹⁷, while the red box marks the area of the excavated basal sequence. **c)** West profile of Layers 12 to 7. The lower part of the large rock that was removed is on top of Layer 7. **b** (inset), adapted from ref. 17.

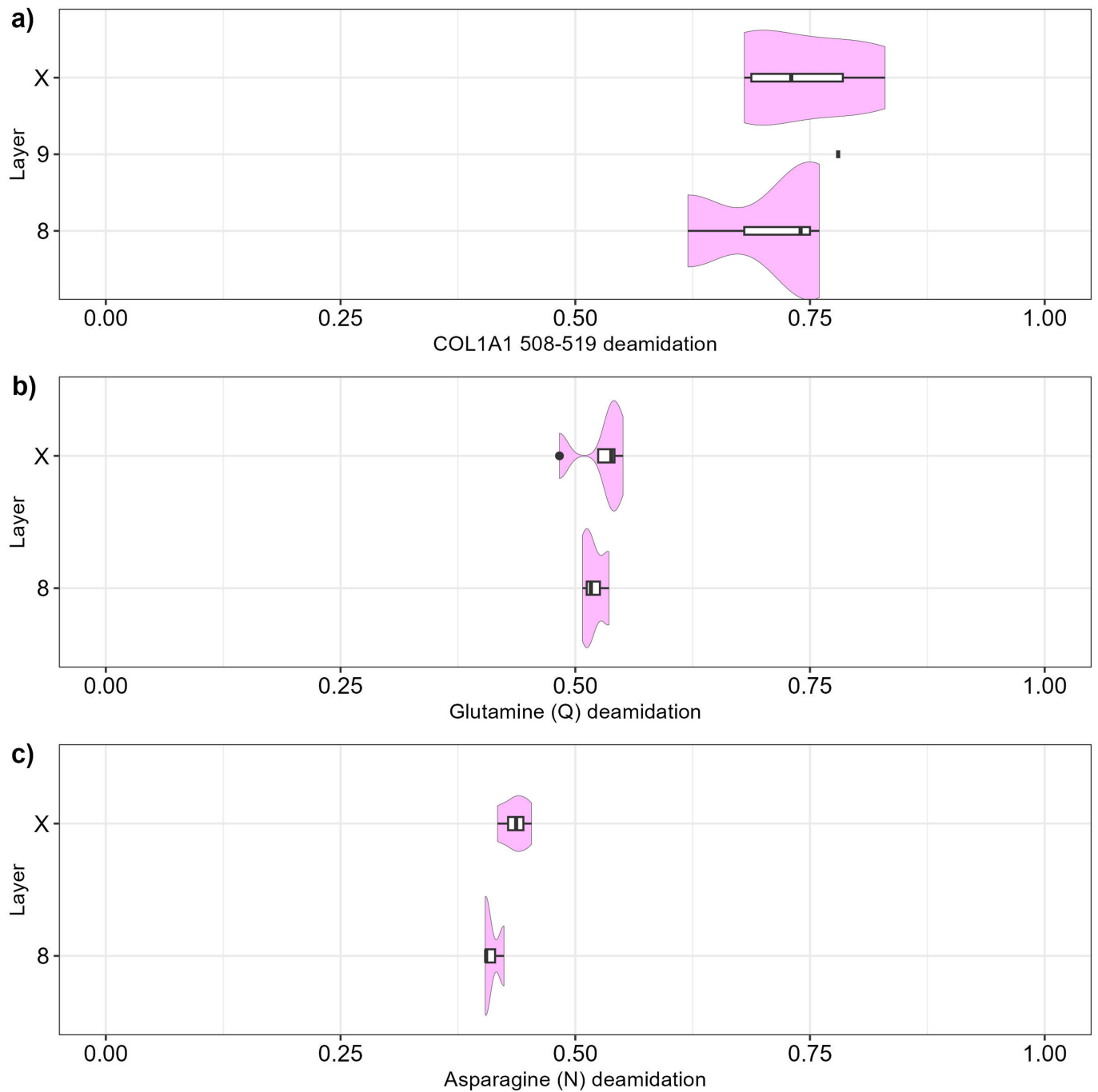


Extended Data Fig. 2 | Map of Ranis with the location of the newly identified hominin specimens and selected lithic artefacts. The numbered squares were excavated by W.M. Hülle in the 1930s and we excavated the blue area between 2016 and 2022. The human specimen IDs are provided on the figure (Tab. S5, S1); the five specimens with an asterisk next to their ID showed no pairwise differences in their mtDNA. The artefact IDs are as follows (from left to right when more than one is present in the same square): sq. 51 - 2, 46^B;

sq. 101/107 - 2, 31^{Pb}, 2, 56^B; sq. 51 A/114 - 2, 32^J, 2, 36^J, 2, 37^J, 2, 52^B, 2, 54^B; sq. 144/154 - 2, 24^J, 2, 29^{Pb}, 2, 42^B, 2, 43^J, 2, 59^J; sq. 164 - 2, 26^J, 2, 60^J, 2, 78^B. Artefacts marked with a^B, J, Pb and B are bifacial leaf points, Jerzmanowice points, pointed blades and a blade, respectively. The illustrated lithic artefacts were all found in the same layers and on the same day as or within a day of the excavation of the newly identified human remains from the same squares. Site map and artefact drawings are modified from Hülle¹⁷.

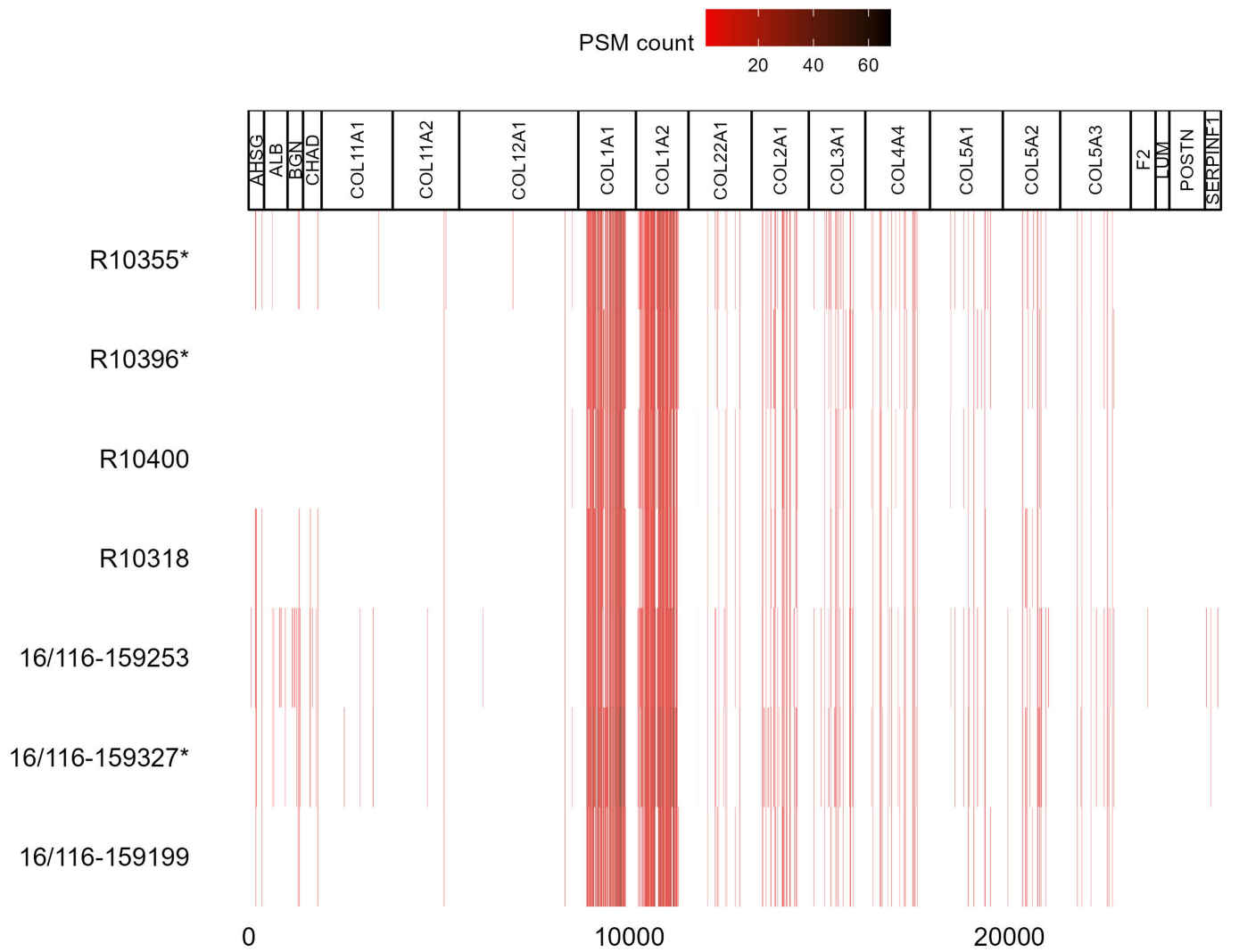


Extended Data Fig. 3 | Chronological site model of 2016-2022 material from Ranis. Directly dated human remains are shown in red, and faunal bones with anthropogenic modifications are shown in green. Along the top of the figure, the North Greenland Ice Core Project (NGRIP) GICC05 $\delta^{18}\text{O}$ curve (dark blue) is shown with warmer Greenland Interstadials (GI17-5) and cooler Greenland Stadial 12 (GS12) and Heinrich Events (HE5, HE4) indicated^{79,80}. Climatic cooling effects correlating with GS12 can also be seen in German palaeoclimate records closer to Ranis: the purple curve shows the *Betula* pollen (%) measured in the Füramoos pollen record from southern Germany⁸¹ and the green curve shows the Total Organic Carbon Content (TOC) in the Eifel maar sediment core in southwestern Germany⁸². Given the errors inherent in the ^{14}C chronology and climate records themselves, any correlations noted here are tentative⁸³. The model outputs are shown in Tab. S15, S1 and further information is in SI section 4.2.



Extended Data Fig. 4 | Protein deamidation for all hominin specimens in Ranis. **a)** Deamidation rate of COL1A1 508–519 for hominin specimens in the 2016–2022 and 1932–1938 excavations with ZooMS (layer X, $n = 4$ NISP; layer 8, $n = 3$; layer 9, $n = 1$), **b)** Glutamine (Q) deamidation plot for hominin specimens in the 2016–2022 and 1932–1938 excavations analysed with directDIA SPIN (layer X, $n = 4$; layer 8, $n = 3$), and **c)** Asparagine (N) deamidation plot for hominin specimens in the 2016–2022 and 1932–1938 excavations analysed with directDIA SPIN (layer X, $n = 4$; layer 8, $n = 3$). The hominin specimen recovered from layer 9

was not included in the SPIN analysis (plots b and c). For panel a, 1 indicates no deamidation of N or Q, while 0 indicates complete deamidation of N or Q. For panels b and c, 0 indicates no deamidation of N or Q, while 1 indicates complete deamidation of N or Q. The box plots within the violin plots define the range of the data (whiskers extend to $1.5 \times$ the interquartile range), outliers (black dots, beyond $1.5 \times$ the interquartile range), 25th and 75th percentiles (boxes), and medians (centre lines).



Extended Data Fig. 5 | Proteomic coverage for the seven hominin bone specimens analysed with SPIN. Peptide spectrum match (PSM) count per protein amino acid for each hominin specimen by libraryDIA of the 20 genes used in R  ther et al.³. White indicates no coverage, red indicates medium

coverage, and black indicates high coverage. The asterisk (*) marks the specimens where mtDNA indicates they originate from the same or maternally related individuals. The x-axis represents the amino acid position in the protein sequence alignment of the 20 proteins considered in SPIN analysis.

Article

Extended Data Table 1 | Hominin specimens identified in Ranis

Specimen ID	Morphological ID	ZooMS ID	SPIN ID	mtDNA	Square	Layer	Excavation
R10355	-	<i>Homo</i>	<i>Homo</i>	<i>Homo sapiens</i>	51A	X	1932-1938
R10396	-	<i>Homo</i>	<i>Homo</i>	<i>Homo sapiens</i>	164	X	1932-1938
R10400	-	<i>Homo</i>	<i>Homo</i>	<i>Homo sapiens</i>	51	X	1932-1938
R10318	-	<i>Homo</i>	<i>Homo</i>	<i>Homo sapiens</i>	51A	X	1932-1938
R10874	<i>Homo</i>	-	-	<i>Homo sapiens</i>	101/102/107	X	1932-1938
R10873	<i>Homo</i>	-	-	<i>Homo sapiens</i>	114	IX-X	1932-1938
R10875	<i>Homo sapiens?</i>	-	-	<i>Homo sapiens</i>	14C	X-XI?	1932-1938
R10876	<i>Homo</i>	-	-	<i>Homo sapiens</i>	19A	X-XI	1932-1938
R10879	<i>Homo?</i>	-	-	<i>Homo sapiens</i>	144/154	X-XI	1932-1938
16/116-159253	-	<i>Homo</i>	<i>Homo</i>	<i>Homo sapiens</i>	1004/999	8	2016-2022
16/116-159327	-	<i>Homo</i>	<i>Homo</i>	<i>Homo sapiens</i>	1003/1000	8	2016-2022
16/116-159199	-	<i>Homo</i>	<i>Homo</i>	<i>Homo sapiens</i>	1003/999	8	2016-2022
16/116-159416	-	<i>Homo</i>	-	<i>Homo sapiens</i>	1003/999	9	2016-2022

Hominin specimens are organised by their recovery during either the 1932–1938 or 2016–2022 excavations.

Reporting Summary

Nature Portfolio wishes to improve the reproducibility of the work that we publish. This form provides structure for consistency and transparency in reporting. For further information on Nature Portfolio policies, see our [Editorial Policies](#) and the [Editorial Policy Checklist](#).

Statistics

For all statistical analyses, confirm that the following items are present in the figure legend, table legend, main text, or Methods section.

n/a	Confirmed
<input type="checkbox"/>	<input checked="" type="checkbox"/> The exact sample size (n) for each experimental group/condition, given as a discrete number and unit of measurement
<input checked="" type="checkbox"/>	<input type="checkbox"/> A statement on whether measurements were taken from distinct samples or whether the same sample was measured repeatedly
<input type="checkbox"/>	<input checked="" type="checkbox"/> The statistical test(s) used AND whether they are one- or two-sided <i>Only common tests should be described solely by name; describe more complex techniques in the Methods section.</i>
<input checked="" type="checkbox"/>	<input type="checkbox"/> A description of all covariates tested
<input type="checkbox"/>	<input checked="" type="checkbox"/> A description of any assumptions or corrections, such as tests of normality and adjustment for multiple comparisons
<input type="checkbox"/>	<input checked="" type="checkbox"/> A full description of the statistical parameters including central tendency (e.g. means) or other basic estimates (e.g. regression coefficient) AND variation (e.g. standard deviation) or associated estimates of uncertainty (e.g. confidence intervals)
<input type="checkbox"/>	<input checked="" type="checkbox"/> For null hypothesis testing, the test statistic (e.g. F , t , r) with confidence intervals, effect sizes, degrees of freedom and P value noted <i>Give P values as exact values whenever suitable.</i>
<input type="checkbox"/>	<input checked="" type="checkbox"/> For Bayesian analysis, information on the choice of priors and Markov chain Monte Carlo settings
<input checked="" type="checkbox"/>	<input type="checkbox"/> For hierarchical and complex designs, identification of the appropriate level for tests and full reporting of outcomes
<input checked="" type="checkbox"/>	<input type="checkbox"/> Estimates of effect sizes (e.g. Cohen's d , Pearson's r), indicating how they were calculated

Our web collection on [statistics for biologists](#) contains articles on many of the points above.

Software and code

Policy information about [availability of computer code](#)

Data collection

Data analysis

For manuscripts utilizing custom algorithms or software that are central to the research but not yet described in published literature, software must be made available to editors and reviewers. We strongly encourage code deposition in a community repository (e.g. GitHub). See the Nature Portfolio [guidelines for submitting code & software](#) for further information.

Data

Policy information about [availability of data](#)

All manuscripts must include a [data availability statement](#). This statement should provide the following information, where applicable:

- Accession codes, unique identifiers, or web links for publicly available datasets
- A description of any restrictions on data availability
- For clinical datasets or third party data, please ensure that the statement adheres to our [policy](#)

The raw mass spectrometry LC-MS/MS proteomics data generated in this study have been deposited to the ProteomeXchange Consortium via the PRIDE partner repository under accession code PDX-043272. The raw mass spectrometry LC-MS/MS and MaxQuant search proteomics data for six bone specimens analyzed in DDA mode included in this study are deposited the ProteomeXchange Consortium via the PRIDE partner repository with the dataset identifier PXD-042321. The

MALDI-TOF .mzml and .msd type files included in this study are available in Zenodo (<https://doi.org/10.5281/zenodo.8063812>). The newly reconstructed mtDNA sequences are available on the DRYAD databases (<https://doi.org/10.5061/dryad.1jwstqk0s>). The sequencing data is available on the European Nucleotide Archive (PRJEB67776). Radiocarbon data is available in the supplementary information.

Research involving human participants, their data, or biological material

Policy information about studies with [human participants or human data](#). See also policy information about [sex, gender \(identity/presentation\), and sexual orientation](#) and [race, ethnicity and racism](#).

Reporting on sex and gender	NA
Reporting on race, ethnicity, or other socially relevant groupings	NA
Population characteristics	NA
Recruitment	NA
Ethics oversight	NA

Note that full information on the approval of the study protocol must also be provided in the manuscript.

Field-specific reporting

Please select the one below that is the best fit for your research. If you are not sure, read the appropriate sections before making your selection.

Life sciences Behavioural & social sciences Ecological, evolutionary & environmental sciences

For a reference copy of the document with all sections, see [nature.com/documents/nr-reporting-summary-flat.pdf](https://www.nature.com/documents/nr-reporting-summary-flat.pdf)

Ecological, evolutionary & environmental sciences study design

All studies must disclose on these points even when the disclosure is negative.

Study description	The Lincombian-Ranisian-Jerzmanowician (LRJ) is an archaeological technocomplex of the Middle to Upper Paleolithic transition spanning from Poland to Britain and whose makers are yet unknown. The main research questions of our project were: who made the LRJ and what is the chronology of their occupation? The site Ilsenhöhle in Ranis is one of the type sites of the LRJ and the target of our investigations. The site was initially excavated from 1932-1938. The collection from this excavation period is stored in the Landesmuseum für Vorgeschichte Halle/Saale, Germany. We excavated the site Ilsenhöhle in Ranis from 2016-2022. The goal was to clarify and date the stratigraphy, and obtain samples from the entire stratigraphy, with a focus on the LRJ find layer. These samples include: sediment samples, artefacts, bones, charcoal and sediment DNA. Additionally, we worked on the 1932-1938 collection and analysed the material. Based on the detailed stratigraphy of the new excavations and the dating, the material of old and new excavations can be correlated.
Research sample	Samples from archaeological fieldwork (sediment including micromorphology and sediment DNA, bones, charcoal, artefacts), and from the collection of the 1932-1938 excavation (bones).
Sampling strategy	For proteomic analysis, 20 mg of fine bone powder was homogenized and equally divided into two different tubes. For radiocarbon dating, samples were selected based on their stratigraphic context and presence of anthropogenic modifications (faunal bones) and human material from both collections was selected for direct dating. ~300-600 mg material was sampled from faunal bones and minimal sampling strategies were employed for the human remains (55-160 mg) to minimise destructive sampling. The amount for genetic analysis s between 9.9 and 63.9 mg per skeletal fragment.
Data collection	Data from the 2016-2022 fieldwork was collected during excavation. The 1932-1938 collection (bones) was provided from the Landesmuseum für Vorgeschichte Halle/Saale, Germany.
Timing and spatial scale	Excavations of Ilsenhöhle in Ranis were conducted from 2016-2022. The sampling of the 1932-1938 collection (bones), stored in the Landesmuseum für Vorgeschichte Halle/Saale was done in parallel to the fieldwork.
Data exclusions	No data were excluded from this study.
Reproducibility	We performed two different types of proteomic analysis (Zooarchaeology by Mass spectrometry and shotgun proteomics) for species identification of a subset of bone specimens. However, not all specimens were analysed by the two different proteomic approaches.
Randomization	Randomization was not relevant to the current study - all available archaeological data were collectively analysed.
Blinding	Blinding was not relevant to the current study - all available archaeological materials were analysed.

Did the study involve field work? Yes No

Field work, collection and transport

Field conditions	The field conditions were optimal and temperate in terms of temperature. We excavated mostly during summer. Weather had only minimal effect as the site is a cave setting and was additionally protected by a roof.
Location	Ilsehöhle in Ranis/ Thuringia, Germany: 50°39.7563'N, 11°33.9139'E
Access & import/export	We had direct access to the site Ilsehöhle in Ranis and the Landesmuseum für Vorgeschichte/ Halle, as all responsible authorities are part of the study.
Disturbance	No disturbance

Reporting for specific materials, systems and methods

We require information from authors about some types of materials, experimental systems and methods used in many studies. Here, indicate whether each material, system or method listed is relevant to your study. If you are not sure if a list item applies to your research, read the appropriate section before selecting a response.

Materials & experimental systems

n/a	Involved in the study
<input checked="" type="checkbox"/>	<input type="checkbox"/> Antibodies
<input checked="" type="checkbox"/>	<input type="checkbox"/> Eukaryotic cell lines
<input type="checkbox"/>	<input checked="" type="checkbox"/> Palaeontology and archaeology
<input checked="" type="checkbox"/>	<input type="checkbox"/> Animals and other organisms
<input checked="" type="checkbox"/>	<input type="checkbox"/> Clinical data
<input checked="" type="checkbox"/>	<input type="checkbox"/> Dual use research of concern
<input checked="" type="checkbox"/>	<input type="checkbox"/> Plants

Methods

n/a	Involved in the study
<input checked="" type="checkbox"/>	<input type="checkbox"/> ChIP-seq
<input checked="" type="checkbox"/>	<input type="checkbox"/> Flow cytometry
<input checked="" type="checkbox"/>	<input type="checkbox"/> MRI-based neuroimaging

Palaeontology and Archaeology

Specimen provenance	Excavation of the site Ilsehöhle in Ranis. Responsible: Thuringian State Office for the Preservation of Historical Monuments and Archaeology, Weimar.
Specimen deposition	Thuringian State Office for the Preservation of Historical Monuments and Archaeology, Weimar, Germany (2016-2022 collection); and Landesamt für Denkmalpflege und Archäologie Sachsen-Anhalt-Landesmuseum für Vorgeschichte, Halle, Germany (1932-1938 collection)
Dating methods	36 new radiocarbon dates are reported (bone = 27, charcoal = 3) from material sampled from the 1932-1938 collection and 2016-2022 collection. Human samples were selected for direct dating and faunal/charcoal material was selected from the new excavation based on stratigraphic context. Animal bones with anthropogenic modifications were selected where possible. ~300-600 mg material was sampled from faunal remains and 55-160 mg from human remains. Bone samples were pretreated at the MPI-EVA (Leipzig, Germany) using an acid-base-acid plus ultrafiltration protocol, with quality assessed based on collagen yield (%) and elemental values derived through EA-IRMS (C%, N%, C:N). Collagen extracts were graphitised and AMS dated at the Laboratory of Ion Beam Physics at ETH-Zurich (Switzerland; lab code ETH). Charcoal samples were pretreated with an ABOx pretreatment method, graphitised and AMS dated at the Curt-Engelhorn-Centre for Archaeometry (Mannheim, Germany; lab code MAMS). Two charcoal dates were excluded from the site model based on their low C% following combustion. All the dates were calibrated using the IntCal20 calibration curve (Reimer et al 2020). Calibration and modelling were done using OxCal (v4.4). All measured and calibrated dates are reported.
<input checked="" type="checkbox"/>	Tick this box to confirm that the raw and calibrated dates are available in the paper or in Supplementary Information.
Ethics oversight	No ethical approval was required for this study considering we did not perform any experiments on living organisms.

Note that full information on the approval of the study protocol must also be provided in the manuscript.